

# Gradient-Informed Machine Learning in Electromagnetics

Matteo Zorzetto<sup>1</sup>, Merle Backmeyer<sup>2</sup>, Michael Wiesheu<sup>2</sup>,  
Riccardo Torchio<sup>1,3</sup>, Fabrizio Dughiero<sup>1</sup>, and Sebastian Schöps<sup>2</sup>

<sup>1</sup>Department of Industrial Engineering, University of Padova, 35131 Padova, Italy

<sup>2</sup>Computational Electromagnetics Group, Technische Universität Darmstadt, 64289 Darmstadt, Germany

<sup>3</sup>Department of Information Engineering, University of Padova, 35131 Padova, Italy

Simulation techniques such as the finite element method are essential for designing electrical devices, but their computational cost can be prohibitive for repeated or real-time computations. Projection-based model order reduction techniques mitigate this by reducing the model size and complexity, yet face challenges when extended to nonlinear or non-affine parametric models. In this work, Isogeometric Analysis (IGA) is combined with proper orthogonal decomposition and Gaussian process regression to construct a non-intrusive surrogate model of a parametric nonlinear model of a permanent magnet synchronous machine. The differentiable nature of IGA allows for computationally efficient extraction of parametric sensitivities, which are leveraged for gradient-enhanced surrogate modeling.

**Index Terms**—Gaussian Process Regression, Proper Orthogonal Decomposition, Isogeometric Analysis, Electromagnetic Modeling.

## I. INTRODUCTION

**S**IMULATION techniques offer powerful tools for analyzing, designing, and monitoring electrical devices. Methods such as the finite element method convert physical equations into large systems of algebraic equations, which can then be solved using numerical linear algebra. However, the computational cost associated with solving these systems can become a limiting factor when repeated computations are required, such as in system-level simulations, design optimization, or real-time control. Projection-based Model Order Reduction (MOR) techniques address this problem by projecting the system matrices onto a lower-dimensional subspace, obtaining a computationally efficient Reduced-Order Model (ROM). Approaches such as balanced truncation, moment matching, and Proper Orthogonal Decomposition (POD) [1], [2] are particularly effective for linear systems and differ by how they find the reduced basis. However, their extension to nonlinear and parametric models is challenging and intrusive [1]. Algorithms such as the discrete empirical interpolation method can treat nonlinear terms [3], [4], [5], but their application requires access to the nonlinear representation of the system, which is not granted, especially when commercial software is involved [6]. Moreover, although projection-based methods can be extended to handle affine parametric dependencies, producing a parametric ROM that preserves the structure of the original model, certain types of dependencies remain difficult to accommodate [1]. In particular, geometric parameter variations often violate the assumptions required for an affine decomposition, making them poorly suited for standard projection-based MOR frameworks. In recent years, machine learning techniques have been increasingly employed to overcome these challenges by learning the relationship between system parameters and quantities of interest directly from data. In this framework, the high-dimensional field variables can be decomposed using methods such as POD [7], [8] or autoen-

coders [9], [10], resulting in a compact set of latent variables that capture the dominant dynamics of the system. Machine learning models such as neural networks [11], radial basis function interpolation [7], and Gaussian process regression (GPR) [6], [9], [8], can then be trained to map the system parameters to this reduced space, enabling the reconstruction of the full-order field with significantly lower computational cost. In this context, Isogeometric Analysis (IGA) offers a significant advantage over the standard finite element method, since we can keep the spatial mapping consistent to enable calculation of gradients. This allows for computationally efficient extraction of the state vector sensitivities with respect to geometric parameters. This derivative information can be leveraged to enhance the surrogate model. It can be incorporated into the reduced basis to construct a more expressive subspace for representing the state vector. Moreover, it can be used within gradient-enhanced interpolation schemes, such as GPR (aka Kriging), to improve the predictive accuracy of the surrogate in the latent space with respect to gradient-free approaches [12]. In this work, the Gradient-Free (GF) IGA approach, previously combined with POD interpolation in [11], is further enhanced by incorporating the Gradient-Enhanced (GE) methodology introduced in [12]. The resulting method is capable of generating accurate surrogate models of electrical devices that include both nonlinear material behavior and geometric parameter variations. The effectiveness of the approach is demonstrated on a permanent-magnet synchronous machine (PMSM) through two studies. First, POD is combined with gradient-enhanced GPR to construct a surrogate model of the electromagnetic field distribution. Moreover, gradient information is directly exploited to build surrogate models for Key Performance Indicators (KPIs) such as torque.

## II. MOTOR MODEL

The method is applied to a PMSM from [13], [14], shown in Figure 1, with fixed rotor position, where the geometric design

Corresponding author: M. Zorzetto

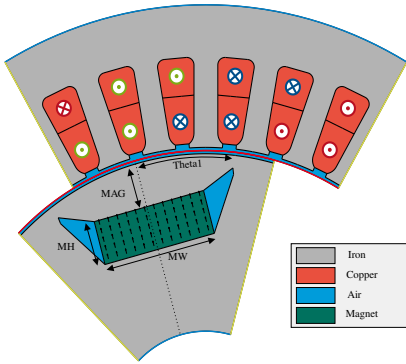


Fig. 1: Parametrization of the PMSM geometry, based on [14].

variables  $\mathbf{p} = [\text{MH}, \text{MW}, \text{MAG}, \text{Theta1}]$  will later be varied for surrogate modeling. The iron cores are shown in gray, the (homogenized) copper slots in red, the rotor magnet in green, and the air gap and air pockets in blue. The physical model is described in detail in [14]. The parameterization is discussed in [11]. For brevity, only the key aspects are outlined here.

### A. Governing Equations

For the laminated PMSM, the parameter-dependent magnetic vector potential in the rotor and stator,  $A_{z,R}$  and  $A_{z,S}$  respectively, is obtained from the two-dimensional magneto-static Poisson problem [15], [16]

$$\nabla \cdot (\nu \nabla A_{z,R}^{(\mathbf{p})}) = \nu \nabla \cdot \mathbf{B}_{\text{rem}}^{\perp (\mathbf{p})} \quad \text{in } \Omega_R^{(\mathbf{p})}, \quad (1)$$

$$\nabla \cdot (\nu \nabla A_{z,S}^{(\mathbf{p})}) = -J_{z,\text{src}} \quad \text{in } \Omega_S^{(\mathbf{p})}, \quad (2)$$

driven by the source current density  $J_{z,\text{src}}$  and the remanent flux density  $\mathbf{B}_{\text{rem}}^{(\mathbf{p})}$  of the permanent magnets, which may also depend on the parameter vector. The reluctivity  $\nu = \nu(\cdot)$  may be non-linear and the magnetic flux density is given by  $\mathbf{B}^{(\mathbf{p})} = \nabla \times (A_z^{(\mathbf{p})} \mathbf{e}_z)$ . Problem (1–2) is complemented with standard boundary conditions, and the coupling across  $\Gamma_{\text{ag}} = \bar{\Omega}_R^{(\mathbf{p})} \cap \bar{\Omega}_S^{(\mathbf{p})}$  is enforced by a Lagrange multiplier and additional coupling conditions (see [17]). The electromagnetic torque is computed from the field solution; thus it also depends on the parametric realization of the problem [15].

### B. IGA Discretization

The discretization of the geometry as well as the solution is performed using Non-Uniform Rational B-Spline basis functions, following the principles of IGA [18]. The physical domain is described by a multi-patch parametrization, decomposing it into a collection of subdomains, each with a corresponding projection map to the same reference domain [19]. Despite different geometrical realizations, the reference domain stays the same, which is essential if the parametric problem is learned in terms of its coefficients. For reasonable parametric changes, no remeshing is required, and the learned coefficients belong to the same nodes in the reference domain which are then mapped to the corresponding physical domain [11]. Problem (1–2) is discretized with B-splines following the standard Ritz-Galerkin approach. The

magnetic vector potential in the reference domain is approximated by

$$A_z^{(\mathbf{p})}(\mathbf{x}) \approx \sum_{i=1}^N B_i^q(\mathbf{p}, \mathbf{x}) u_i \quad (3)$$

where  $u_i$  are the unknown coefficients and  $B_i^q(\mathbf{p}, \mathbf{x})$  are the spline basis functions of degree  $q$ . The physical problem results in a nonlinear system of equations dependent on the geometrical parameters  $\mathbf{p}$ :

$$\mathbf{A}(\mathbf{p}, \mathbf{u}) \mathbf{u} = \mathbf{b}, \quad (4)$$

where  $\mathbf{u}$  is the state vector, including variables for the rotor and stator, as well as Lagrange multipliers for rotor-stator coupling.

$\mathbf{A}(\mathbf{p}, \mathbf{u})$  is assembled with stiffness matrices and coupling terms that depend on geometrical parameters and the state vector due to the presence of nonlinear materials. The vector  $\mathbf{b}$  describes the excitations of rotor and stator that are given by the permanent magnet and the coils. For more details on constructing the matrix system (4) the reader is referred to [16]. As outlined in [16], analytical computation of the gradients is feasible through the adjoint method. Our implementation of IGA [20] not only provides the solution vector  $\mathbf{u}(\mathbf{p}_*)$  but also enables efficient evaluation of its sensitivities with respect to each component of  $\mathbf{p}$ :  $\partial_1 \mathbf{u}(\mathbf{p}_*), \dots, \partial_{n_p} \mathbf{u}(\mathbf{p}_*)$ , which will be leveraged for surrogate modeling in the following.

## III. SURROGATE MODELING

The surrogate modeling approach employed in this work consists of two main components: POD, used to obtain a low-dimensional representation of the solution fields, and GPR, used to model the dependence of the reduced coefficients on the parameters. Following [12], both POD and GPR are enriched with gradient information from the IGA model to improve accuracy.

### A. Proper Orthogonal Decomposition

POD finds a reduced representation of the solution starting from the snapshot matrix, obtained by concatenating a set of solutions of the problem:

$$\mathbf{U} = [\mathbf{u}(\mathbf{p}_1), \dots, \mathbf{u}(\mathbf{p}_{n_s})] \in \mathbb{R}^{n \times n_s}, \quad (5)$$

where  $n$  is the number of degrees of freedom, while  $n_s$  is the number of samples in the set. The main assumption behind POD is that the solution vector can be approximated by a linear combination of  $r \ll n$  basis vectors  $\phi$ , which multiply parametric dependent coefficients  $\xi(\mathbf{p})$ . The reduced basis  $\mathbf{Q} = [q_1, \dots, q_r] \in \mathbb{R}^{n \times r}$  is commonly obtained by taking the first  $r$  left singular vectors from the Singular Value Decomposition (SVD) of  $\mathbf{U}$ . Following [11], POD is performed with a weighted inner product obtained via a weighting matrix  $\bar{\mathbf{A}} = \mathbf{A}(\bar{\mathbf{p}}, \mathbf{0})$ , chosen as the system matrix from Equation 4, evaluated with homogeneous unit material at the expected parameter combination  $\bar{\mathbf{p}}$ . Although  $\mathbf{A}$  depends on the parameters, it is kept constant to simplify the basis computation. With this weighted inner product, the POD modes are obtained by solving the generalized eigenvalue problem

$$\mathbf{U}^T \bar{\mathbf{A}} \mathbf{U} \phi_i = \lambda_i \phi_i, \quad i = 1, \dots, r, \quad (6)$$

and defining the reduced basis vectors as

$$\mathbf{q}_i = \frac{1}{\sqrt{\lambda_i}} \mathbf{U} \phi_i, \quad i = 1, \dots, r. \quad (7)$$

The reduced coefficients can then be found for a generic parameter combination  $\mathbf{p}^*$  by

$$\boldsymbol{\xi}(\mathbf{p}^*) = \mathbf{Q}^T \bar{\mathbf{A}} \mathbf{u}(\mathbf{p}^*). \quad (8)$$

Truncating the basis at a fixed value  $r$  introduces a reconstruction error, which can be monitored by:

$$\epsilon_{\text{rel}}^2 = \frac{(\mathbf{u} - \mathbf{Q} \boldsymbol{\xi})^T \mathbf{A} (\mathbf{u} - \mathbf{Q} \boldsymbol{\xi})}{\mathbf{u}^T \mathbf{A} \mathbf{u}}. \quad (9)$$

After dimensionality reduction, machine learning approaches such as GPR can be used to find a function  $f$ , mapping  $\mathbf{p}$  to  $\boldsymbol{\xi}$ , from which the field distribution can be reconstructed by:

$$\mathbf{u}(\mathbf{p}^*) \approx \tilde{\mathbf{u}}(\mathbf{p}^*) = \mathbf{Q} \boldsymbol{\xi}, \quad \boldsymbol{\xi} \approx \mathbf{f}(\mathbf{p}^*) \quad (10)$$

If gradient information is available, a more general POD basis can be derived by augmenting the snapshot matrix  $\mathbf{U}$  [12]:

$$\mathbf{U}_{\text{aug}} = [\mathbf{u}(\mathbf{p}_1), \mathbf{u}_1(\mathbf{p}_1), \dots, \mathbf{u}_{n_p}(\mathbf{p}_1), \dots, \mathbf{u}_{n_p}(\mathbf{p}_{n_s})], \quad (11)$$

where  $n_p$  is the number of parameters and  $\mathbf{u}_i(\mathbf{p}_j)$  stands for [12]:

$$\mathbf{u}_i(\mathbf{p}_j) = \mathbf{u}(\mathbf{p}_j) + h \cdot \frac{\partial \mathbf{u}}{\partial p_i}(\mathbf{p}_j). \quad (12)$$

where  $h$  is a small value, chosen here to be  $10^{-3}$ .

### B. Gaussian Process Regression

This section briefly outlines GPR and its extension to the gradient-enhanced case. A more detailed presentation can be found in [21]. A Gaussian process  $\mathcal{GP}$  is a distribution over functions and is defined by a mean function  $\mu(\mathbf{x})$  and a covariance function  $k(\mathbf{x}, \mathbf{x}')$  [21] as

$$f(\mathbf{x}) \sim \mathcal{GP}(\mu(\mathbf{x}), k(\mathbf{x}, \mathbf{x}')), \quad (13)$$

where the mean function

$$\mu(\mathbf{x}) = \mathbb{E}[f(\mathbf{x})] \quad (14)$$

represents the expected function value for input  $\mathbf{x}$ , while the covariance function

$$k(\mathbf{x}, \mathbf{x}') = \mathbb{E}[(f(\mathbf{x}) - \mu(\mathbf{x}))(f(\mathbf{x}') - \mu(\mathbf{x}'))] \quad (15)$$

models the relationship between function values at different input points  $\mathbf{x}$  and  $\mathbf{x}'$  [21], [22]. A set of observations  $\mathbf{X}_t, \mathbf{y}_t$ , corresponding in this work to the parameter vector  $\mathbf{p}$  and the reduced coefficients  $\boldsymbol{\xi}$  respectively, is collected, and a kernel, such as the radial basis function, is chosen:

$$k(\mathbf{x}, \mathbf{x}') = \sigma_f^2 \exp\left(-\frac{\|\mathbf{x} - \mathbf{x}'\|^2}{2\lambda^2}\right), \quad (16)$$

where  $\sigma_f$  is the signal variance and  $\lambda$  is the length scale. Assuming zero mean, the function value for an unseen input  $\mathbf{x}_*$  can then be obtained by computing the posterior mean of the distribution:

$$\mu(\mathbf{x}_*) = \mathbf{K}(\mathbf{x}_*, \mathbf{X}_t) [\mathbf{K}(\mathbf{X}_t, \mathbf{X}_t) + \sigma_\epsilon^2 \mathbf{I}]^{-1} \mathbf{y}_t, \quad (17)$$

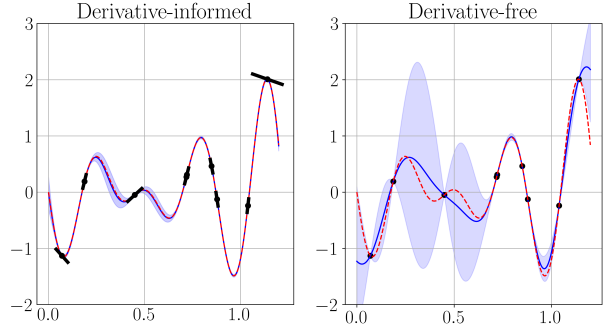


Fig. 2: Gradient enhanced GPR for a one-dimensional function. Black markers indicate the samples of the true function (represented by the dashed red line) used to fit the models. Blue lines correspond to the prediction, while the shaded area is the 95% confidence interval.

where  $\sigma_\epsilon^2$  is the assumed noise level of the observations,  $\mathbf{I}$  is the identity matrix and entries in the covariance matrices  $\mathbf{K}$  are defined by evaluating the kernel function

$$\mathbf{K}(\mathbf{X}_a, \mathbf{X}_b) = \{k(\mathbf{x}_i^a, \mathbf{x}_j^b)\}_{ij}, \quad (18)$$

where  $\mathbf{X}_a$  and  $\mathbf{X}_b$  represent arbitrary sets of input points. One of the main advantages of GPR compared to other interpolation approaches is the availability of a confidence interval, which can be estimated by the variance function

$$\begin{aligned} \sigma^2(\mathbf{x}_*) &= k(\mathbf{x}_*, \mathbf{x}_*) \\ &\quad - \mathbf{K}(\mathbf{x}_*, \mathbf{X}_t) [\mathbf{K}(\mathbf{X}_t, \mathbf{X}_t) + \sigma_\epsilon^2 \mathbf{I}]^{-1} \mathbf{K}(\mathbf{X}_t, \mathbf{x}_*). \end{aligned} \quad (19)$$

The extension of GPR to the gradient-enhanced case, is performed by modeling the solution and its partial derivatives jointly. For each training point  $\mathbf{x}_*$  the solution is extended from  $y_* = f(\mathbf{x}_*)$  to

$$\mathbf{y}_* = \left[ f(\mathbf{x}_*), \frac{\partial f(\mathbf{x}_*)}{\partial x_i}, \dots, \frac{\partial f(\mathbf{x}_*)}{\partial x_{n_p}} \right]. \quad (20)$$

Matrix  $\mathbf{K}$  is then modified to now include entries corresponding to the covariance between function values  $k(\mathbf{x}, \mathbf{x}')$ , covariance between function values and each partial derivative

$$\frac{\partial k(\mathbf{x}, \mathbf{x}')}{\partial \mathbf{x}}, \quad (21)$$

and covariance between partial derivatives [23]:

$$\frac{\partial^2 k(\mathbf{x}, \mathbf{x}')}{\partial \mathbf{x} \partial \mathbf{x}'}. \quad (22)$$

In Fig. 2, the standard GPR is compared to the gradient-enhanced version for modeling a simple one-dimensional function. As expected, the added derivative information improves the function estimate and tightens the confidence bounds.

## IV. RESULTS

A parametrized IGA model of the geometry in Fig. 1 was developed, discretizing the physical equations into a nonlinear system of 6177 variables, which is a function of the geometrical parameters presented in Table I. Sobol sampling

TABLE I: Parameter bounds

Name	unit	lower bound	upper bound
MH	mm	2	12
MW	mm	8	22
MAG	mm	5	15
Theta1	°	15	23

TABLE II: Times for dataset generation and model fitting in seconds for different dataset partitions.

$n_s$	15	31	61	119
Simulation time	143	295	581	1134
GFGPR (field)	10.3	9.5	8.8	10.8
GEGPR (field)	22.3	25.6	52	82.1
GFGPR (torque)	4.4	2.5	2.5	2.6
GEGPR (torque)	2.6	2.8	4.9	8.1

was employed to generate training datasets of increasing size in order to monitor the accuracy of the approach in data-scarce conditions, removing solutions for which the geometry is too skewed or the magnet exceeds the bounds. The model was simulated on a workstation equipped with a 3.10 GHz Intel® Xeon® processor, with an average time of 10 seconds per datapoint. All partitions, showcased in Table II were tested on the same collection of 30 unseen combinations.

### A. Field Decomposition

For each dataset partition, the standard and augmented snapshot matrices were realized according to (5) and (11). To compare the two approaches, their accuracy was evaluated by monitoring the average relative  $L_2$  error of the magnetic flux density through (9) over the test dataset, computed using  $\bar{\mathbf{A}}$ . In Fig. 3, the relative error is presented for the POD basis trained on the smallest dataset of 15 samples. In this scenario, the augmented snapshot matrix allows for an increased basis size without requiring additional physical samples, thus leading to a smaller reconstruction error. It should be noted, though, that a rank of 14 constitutes an edge case where the training data is perfectly recovered, while generalization to new samples is not guaranteed. In contrast, as presented in Fig. 4, as the number of available samples grows, an improvement in the reconstruction error begins to appear for truncations close to  $n_s$ . This is attributed to information redundancy in the non-augmented dataset, which limits generalization when  $r$  is close to  $n_s$ . The goal of MOR is to obtain an accurate but compact model, discouraging the choice of large truncations  $r$ . Given this consideration, for this test case, augmenting the snapshot matrix provides a marginal improvement in accuracy only for the smallest dataset. For this reason, the standard POD basis was employed in all scenarios, fixing the number of modes to 14, ensuring a fair comparison for the following latent-space modeling.

### B. Field reconstruction

Using the POD basis, the reduced coefficients  $\xi(\mathbf{p}^*)$  and their sensitivities are obtained for all parameter combinations in the training dataset. For each component of  $\xi$ , two separate GPR models (GF and GE) are trained to map the parameter space to the corresponding reduced coefficient. Models are

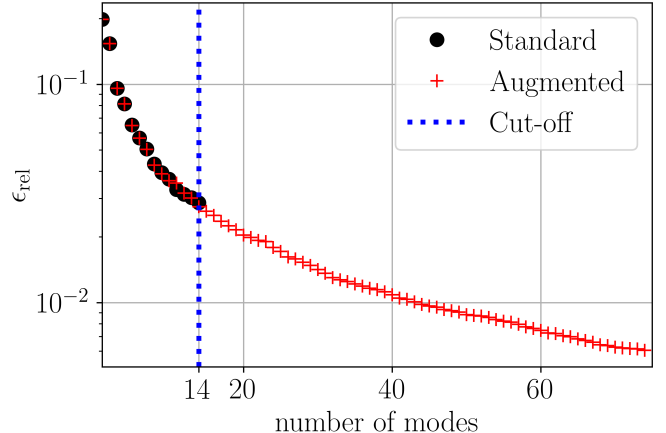


Fig. 3: Average relative  $L_2$  reconstruction error of the magnet flux density for the gradient-free and gradient-enhanced basis for  $n_s = 15$ .

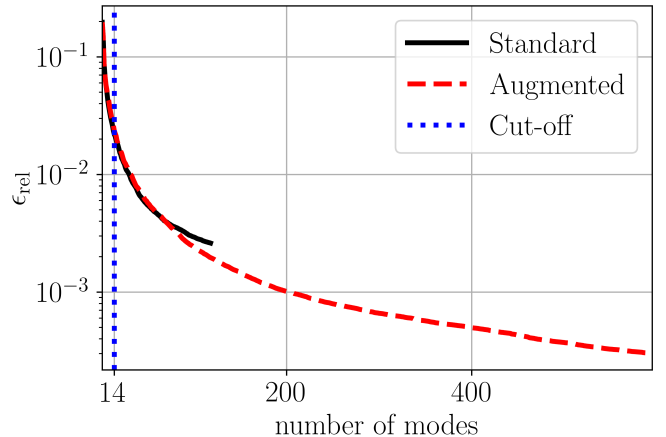


Fig. 4: Average relative  $L_2$  reconstruction error of the magnet flux density for the gradient-free and gradient-enhanced basis for  $n_s = 119$ .

trained using the L-BFGS optimizer with 800 iterations and 3 restarts using GPyTorch [24]. The two surrogate models are then compared by predicting the reduced coefficients  $\tilde{\xi}(\mathbf{p})$  starting from the parameter combinations in the test dataset. These predictions are subsequently used to reconstruct the full field solution  $\tilde{\mathbf{u}}(\mathbf{p})$  via (10) and the relative error if the magnetic flux density is computed through (9), updating  $\mathbf{A}$  for each parameter combination. As shown in Fig. 5, increasing the number of training samples improves the accuracy of both the GF and GE models, with their errors approaching the POD reconstruction error, which constitutes a baseline for the model accuracy. This indicates that the reduced coefficients  $\xi$  are predicted with high accuracy and that the remaining error is primarily due to the POD truncation. The GE approach consistently outperforms the GF method, particularly in data-scarce regimes, motivating the use of gradient information for latent-space modeling. However, as reported in Table II, this improved accuracy comes at the cost of increased training time due to the higher model complexity.

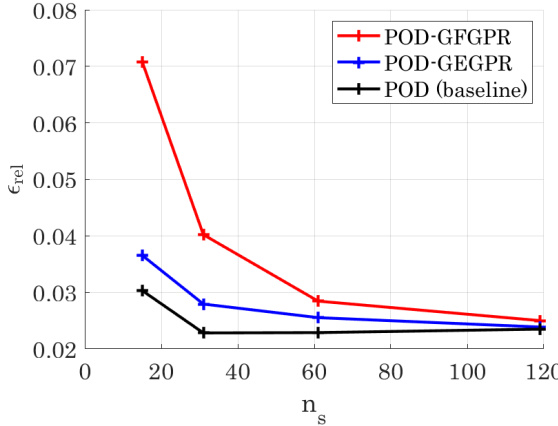


Fig. 5: Average relative  $L_2$  error of the magnetic flux density for gradient-free and gradient-enhanced GPR as a function of the number of samples in the training dataset, compared to the reconstruction error of POD.

### C. KPI prediction

When the objective of surrogate modeling is limited to the prediction of KPIs such as torque, two approaches can be followed. From the full-field surrogate model obtained in subsection IV-B, KPIs can be calculated. Alternatively, they can be modeled directly as a function of the parameters using GPR, possibly by exploiting the availability of torque sensitivities with respect to the parameters, which are readily obtained from the IGA model. Both the GF and GE GPR models were trained for torque prediction, comparing the Mean Absolute Percentage Error (MAPE) Fig. 6. Results indicate that, while both methods yield accurate predictions, directly learning the parameter-to-torque map leads to superior accuracy when gradient information is available, particularly in data-rich regimes where the field reconstruction error becomes the limitation of POD-GPR. In addition, this direct approach eliminates the need to store or construct the full IGA model, resulting in a more compact surrogate representation. Moreover, since only one output is required, as presented in Table II, the training time is also decreased. Ultimately, this comparison is application-dependent, as it is influenced by the smoothness of the KPI and the reduced coefficients with respect to the parameter space, the truncation error, and the number of desired KPIs.

## V. CONCLUSION

In this work, the differentiable nature of Isogeometric Analysis (IGA), enabling the efficient calculation of fields, Key Performance Indicators (KPIs), and their parametric sensitivities, is leveraged for efficient surrogate modeling of electric devices. Proper orthogonal decomposition is employed for dimensionality reduction while gradient-enhanced Gaussian Process Regression (GPR) learns a mapping between parameters and field coefficients to generate surrogate models for the magnetic flux density distribution. Moreover, GPR is also used for parametric surrogate modeling of KPIs. The approach is assessed on a parametric model of a permanent magnet

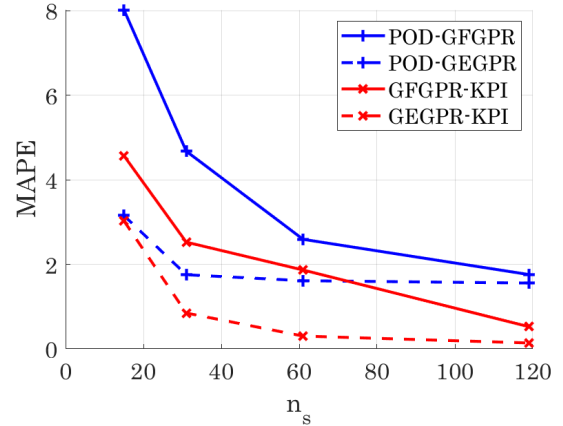


Fig. 6: MAPE of the torque prediction from the gradient-free and gradient-enhanced POD-GPR models compared with GPR performed directly on the KPI.

synchronous motor, considering both data-scarce and data-rich regimes. Results show how, for both the magnetic flux density and the motor torque, including gradient information in the surrogate models significantly improves the model quality, especially in data-scarce regimes. Moreover, the surrogate models reduce evaluation times from tens of seconds for the full IGA simulations to milliseconds, while maintaining high predictive accuracy. Given the short training times and the very fast prediction of new solutions, this approach represents a promising tool for the parametric surrogate modeling of electric devices.

## ACKNOWLEDGMENT

This work was made possible by a scholarship from the German Academic Exchange Service (DAAD), through the program Research Grants in Germany, 2025 (57742125). The work is also supported by the joint DFG/FWF Collaborative Research Centre CREATOR (DFG: Project-ID 492661287/TRR 361; FWF: 10.55776/F90) at TU Darmstadt, TU Graz, and JKU Linz.

## REFERENCES

- [1] P. Benner, S. Gugercin, and K. Willcox, “A Survey of Projection-Based Model Reduction Methods for Parametric Dynamical Systems,” *SIAM Review*, vol. 57, pp. 483–531, Jan. 2015.
- [2] A. Chatterjee, “An introduction to the proper orthogonal decomposition,” *Current Science*, vol. 78, no. 7, pp. 808–817, 2000.
- [3] S. Chaturantabut and D. C. Sorensen, “Nonlinear Model Reduction via Discrete Empirical Interpolation,” *SIAM Journal on Scientific Computing*, vol. 32, pp. 2737–2764, Jan. 2010.
- [4] T. Henneton and S. Clénet, “Model-Order Reduction of Multiple-Input Non-Linear Systems Based on POD and DEI Methods,” *IEEE Transactions on Magnetics*, vol. 51, pp. 1–4, Mar. 2015.
- [5] M. Zorzetto, R. Torchio, F. Lucchini, S. Massei, L. Robol, and F. Dughiero, “Reduced Order Modeling for Thermal Simulations of Electric Components With Surface-to-Surface Radiation,” *IEEE Access*, vol. 12, pp. 178117–178126, 2024.
- [6] G. Ortali, N. Demo, G. Rozza, Mathematics Area, mathLab, SISSA, via Bonomea 265, I-34136 Trieste, Italy, and Department of Applied Physics, Eindhoven University of Technology, The Netherlands, “A Gaussian Process Regression approach within a data-driven POD framework for engineering problems in fluid dynamics,” *Mathematics in Engineering*, vol. 4, no. 3, pp. 1–16, 2021.

- [7] T. Henneron, A. Pierquin, and S. Clénet, “Surrogate Model Based on the POD Combined With the RBF Interpolation of Nonlinear Magnetostatic FE Model,” *IEEE Transactions on Magnetics*, vol. 56, pp. 1–4, Jan. 2020.
- [8] M. Zorzetto, R. Torchio, F. Lucchini, M. Forzan, and F. Dughiero, “Proper Orthogonal Decomposition for Parameterized Macromodeling of a Longitudinal Electromagnetic Levitator,” *IEEE Transactions on Magnetics*, vol. 61, pp. 1–7, Apr. 2025.
- [9] M. Zorzetto, R. Torchio, F. Lucchini, P. D. Barba, M. E. Mognaschi, M. Forzan, and F. Dughiero, “Machine learning-based reduced order modeling of nonlinear and multiphysics magnetic devices,” *IEEE Transactions on Magnetics*, pp. 1–1, 2025.
- [10] F. Pichi, B. Moya, and J. S. Hesthaven, “A graph convolutional autoencoder approach to model order reduction for parametrized PDEs,” *Journal of Computational Physics*, vol. 501, p. 112762, Mar. 2024.
- [11] M. Backmeyer, M. Wiesheu, and S. Schöps, “Learning electromagnetic fields based on finite element basis functions,” *IEEE Transactions on Magnetics*, pp. 1–1, 2025.
- [12] R. Zimmermann, “Gradient-enhanced surrogate modeling based on proper orthogonal decomposition,” *Journal of Computational and Applied Mathematics*, vol. 237, pp. 403–418, Jan. 2013.
- [13] U. Pahner, *A General Design Tool for the Numerical Optimisation of Electromagnetic Energy Transducers*. Phd thesis, KU Leuven, Leuven, 05 1998.
- [14] T. Komann, M. Wiesheu, S. Ulbrich, and S. Schöps, “Robust design optimization of electric machines with isogeometric analysis,” *Math.*, vol. 12, 04 2024.
- [15] S. J. Salon, *Finite Element Analysis of Electrical Machines*. Kluwer, 1995.
- [16] M. Wiesheu, T. Komann, M. Merkel, S. Schöps, S. Ulbrich, and I. Cortes Garcia, “Combined parameter and shape optimization of electric machines with isogeometric analysis,” *Optim. Eng.*, 08 2024. arxiv:2311.06046.
- [17] H. Egger, M. Harutyunyan, R. Löscher, M. Merkel, and S. Schöps, “On torque computation in electric machine simulation by harmonic mortar methods,” *J. Math. Ind.*, vol. 12, no. 6, 2022. arxiv:2112.05572.
- [18] A. Buffa, G. Sangalli, and R. Vázquez, “Isogeometric analysis in electromagnetics: B-splines approximation,” *Comput. Meth. Appl. Mech. Eng.*, vol. 199, pp. 1143–1152, 2010.
- [19] A. Buffa, R. Vázquez Hernández, G. Sangalli, and L. Beirão da Veiga, “Approximation estimates for isogeometric spaces in multipatch geometries,” *Numer. Meth. Part. Differ. Equat.*, vol. 31, no. 2, pp. 422–438, 2015.
- [20] M. Backmeyer, M. Wiesheu, and S. Schöps, “MotorLearning: Version paper with training data.” Zenodo, 11 2025.
- [21] E. Schulz, M. Speekenbrink, and A. Krause, “A tutorial on Gaussian process regression: Modelling, exploring, and exploiting functions,” *Journal of Mathematical Psychology*, vol. 85, pp. 1–16, Aug. 2018.
- [22] T. J. Santner, B. J. Williams, and W. I. Notz, *The Design and Analysis of Computer Experiments*. Springer Series in Statistics, New York, NY: Springer New York, 2018.
- [23] C. E. Rasmussen and C. K. I. Williams, “Gaussian Processes for Machine Learning,” in *Gaussian Processes for Machine Learning*, Adaptive Computation and Machine Learning, pp. 189–198, Cambridge, Mass.: MIT Press, 3. print ed., 2008.
- [24] J. R. Gardner, G. Pleiss, D. Bindel, K. Q. Weinberger, and A. G. Wilson, “Gpytorch: Blackbox matrix-matrix gaussian process inference with gpu acceleration,” in *Advances in Neural Information Processing Systems*, 2018.